

Reflective Dielectric Cavity Enhanced Emission from Hexagonal Boron Nitride Spin Defect Arrays

Xiao-Dong Zeng,^{1,2} Yuan-Ze Yang,^{1,2} Nai-Jie Guo,^{1,2} Zhi-Peng Li,^{1,2} Zhao-An Wang,^{1,2}
Lin-Ke Xie,^{1,2} Shang Yu,^{1,2} Yu Meng,^{1,2} Qiang Li,^{1,2} Jin-Shi Xu,^{1,2,3} Wei Liu,^{1,2,*}
Yi-Tao Wang,^{1,2,†} Jian-Shun Tang,^{1,2,3,‡} Chuan-Feng Li,^{1,2,3,§} and Guang-Can Guo^{1,2,3}

¹CAS Key Laboratory of Quantum Information, University of Science and Technology of China, Hefei, Anhui 230026, China

²CAS Center For Excellence in Quantum Information and Quantum Physics,
University of Science and Technology of China, Hefei, Anhui 230026, China

³Hefei National Laboratory, University of Science and Technology of China, Hefei, Anhui 230088, China

Among the various kinds of spin defects in hBN, the negatively charged boron vacancy (V_B^-) spin defect that can be deterministically generated is undoubtedly a potential candidate for quantum sensing, but its low quantum efficiency restricts its practical applications. Here, we demonstrate a robust enhancement structure with advantages including easy on-chip integration, convenient processing, low cost and suitable broad-spectrum enhancement for V_B^- defects. In the experiment, we used a metal reflective layer under the hBN flakes, filled with a transition dielectric layer in the middle, and adjusted the thickness of the dielectric layer to achieve the best coupling between the reflective dielectric cavity and the hBN spin defect. Using a reflective dielectric cavity, we achieved a PL enhancement of approximately 7-fold, and the corresponding ODMR contrast achieved 18%. Additionally, the oxide layer of the reflective dielectric cavity can be used as an integrated material for micro-nano photonic devices for secondary processing, which means that it can be combined with other enhancement structures to achieve stronger enhancement. This work has guiding significance for realizing the on-chip integration of spin defects in two-dimensional materials.

Introduction

Solid-state optically addressable spin defects are highly sought-after quantum systems for realizing quantum information processing [1–5]. The well-known systems are color centers in diamond [6, 7], silicon carbide [8, 9] and two-dimensional (2D) materials [10, 11]. 2D materials are layered structures, whose layers are connected by van der Waals (vdW) forces. This quantum confinement effect perpendicular to the 2D plane results in many unique properties that are significantly different from those in bulk materials. Hexagonal boron nitride (hBN) is a wide-bandgap (~ 6 eV) 2D material, possessing good transferability and easy integration [12, 13]. Recent studies have shown the existence of color centers in hBN capable of spin initialization, readout, and coherent manipulation at room temperature [14–19].

The most studied spin defect in hBN is the negatively charged boron vacancy (V_B^-) defect, which can exist stably at room temperature [20, 21] and can be deterministically generated in various ways, including neutron irradiation [18], electron beam irradiation [22], focused ion beam (FIB) irradiation [23, 24], laser ablation [25, 26], etc. Experiments have shown that the V_B^- defect a packet spectrum peaked at approximately 810 nm and a nonobvious zero phonon line (ZPL) even at low temperature [25]. Recently, some researchers have shown that the ZPL of V_B^- is at 773 nm through Purcell enhancement

from the photonic crystal cavity [27], which is consistent with the theoretical results [28, 29]. The electron spin orientation of the V_B^- defect is out-of-plane relative to the lattice of hBN, whose ground state and excited state are triplet states. Previous works indicate that V_B^- has a ground-state splitting energy of ~ 3.5 GHz [30] and an excited-state splitting energy of ~ 2.1 GHz [31–34]. Experiments have shown that hBN has great potential in sensing the measurement of temperature [35, 36], stress [37] and magnetic fields [38, 39]. However, the poor quantum efficiency of V_B^- limits the sensitivity to external fields and hinders finding the single V_B^- spin [29].

To enhance the photoluminescence (PL) intensity of V_B^- defects, many methods have been applied, such as photonic crystal cavities [27], plasmonic cavities [40, 41], bullseye cavities [42], and strain engineering [43]. Photonic crystal cavities are suitable for narrow-band, local enhancement, and have significant advantages in on-chip applications, but fabrication of photonic crystal cavities requires complex technology. In addition, there is a coupling problem between the color centers and the photonic crystal cavity [44]. The enhancement effect of metal plasmons is remarkable and the experimental feasibility is high, but the strong coupling interaction between metals and 2D materials can seriously interfere with the PL spectra of 2D materials, making it difficult to analyze the natural properties of 2D materials [45]. Furthermore, some of these methods have limitations considering the strength of microwave radiation, resulting in low optically detected magnetic resonance (ODMR) contrast.

In this paper, a reflective dielectric cavity (RDC) with convenient processing technology and strong scalability is used to enhance the PL intensity of V_B^- spin defects in hBN. The RDC consisting of microwave coplanar wave-

*Email: lw691225@ustc.edu.cn

†Email: yitao@ustc.edu.cn

‡Email: tjs@ustc.edu.cn

§Email: cfli@ustc.edu.cn

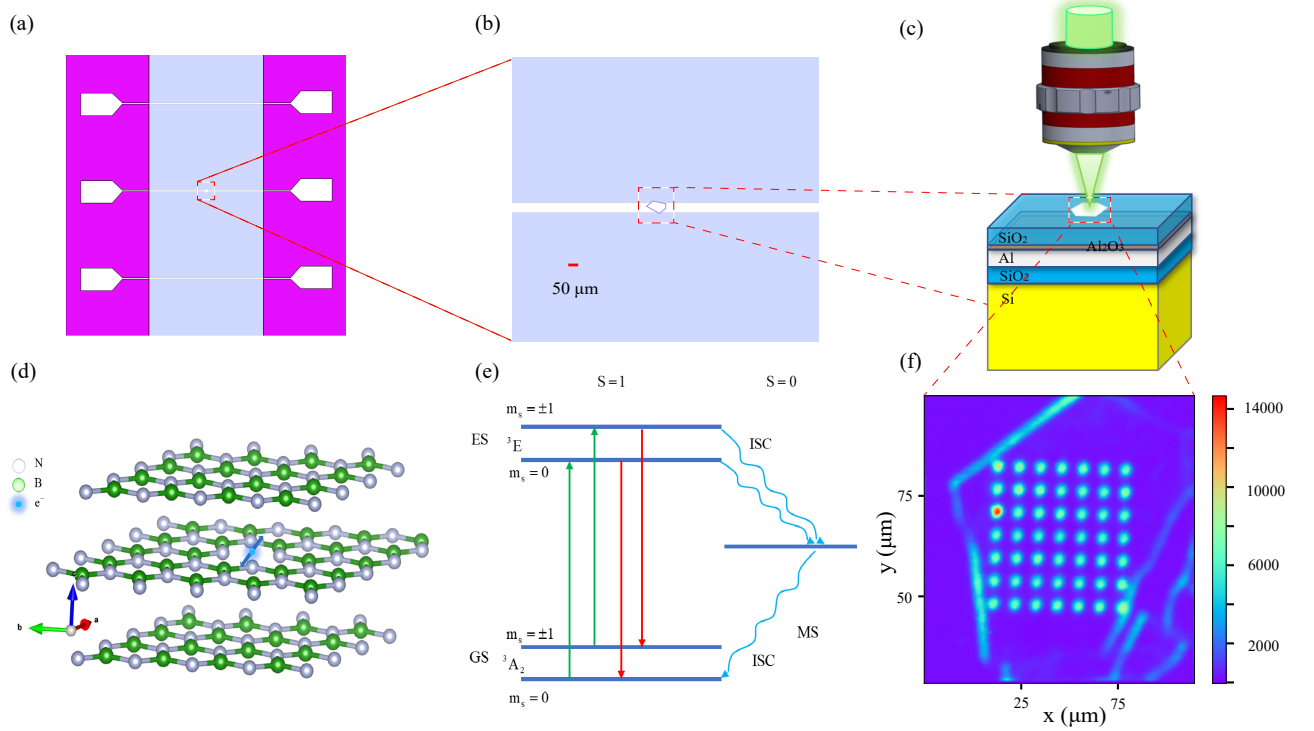


Figure 1. Reflective dielectric cavity structure and V_B^- spin defect energy level structure. (a) Schematic diagram of the coplanar waveguide substrate of the dielectric cavity, obtained from the processing of the SiO_2/Si substrate, and the sample is transferred to the top of the waveguide. (b) The sample is located above the position of the waveguide enlarged, with a waveguide width of $50\text{-}\mu\text{m}$. (c) The hierarchy of the reflective dielectric cavity, from bottom to top, including $500\text{-}\mu\text{m}$ Si layer, 285-nm SiO_2 layer, 115-nm Al layer, 5-nm Al_2O_3 layer, and SiO_2 layer as an isolation medium. (d) Schematic of a V_B^- defect in hBN, where the boron atom is replaced by an electron. (e) Energy level structure diagram of the V_B^- spin defect, whose zero-field splitting (ZFS) of the ground state is approximately 3.5 GHz. (f) The hBN on the reflective dielectric cavity substrate was implanted with helium ions using HIM to generate a photoluminescence array of V_B^- spin defects. The excitation light was a 532-nm laser with a power of 4 mW.

guides as a metal reflector and SiO_2 as a dielectric layer has been used for Raman and PL enhancement of other 2D materials, fluorescent nanodiamonds, and quantum dot reinforcement [45–47]. Combining V_B^- defects with this structure, not only are the fluorescence counts enhanced 7 times but also the ODMR contrast reaches 18%. This structure does not require complex micro-nano fabrication, and it is scalable and effective. In addition, the structure can be used to search for a single spin color center combined with other enhancement structures.

Results

As shown in Figure 1(a), we made aluminum (Al) electrodes as metal reflectors on the SiO_2/Si substrate and coated SiO_2 as a dielectric layer. Subsequently, we transferred the flake hBN to the prepared RDC, and we deterministically generated the V_B^- spin defect array using a helium ion microscope (HIM) with an implantation dose of 1×10^{17} ions/ cm^2 and an implantation energy of 30 KeV. We scanned the PL map of V_B^- spin defects using a home-made confocal microscope as shown in Figure 1(f)

(see Methods for details). Figure 1(c) shows the basic structure of the RDC, including the SiO_2/Si substrate, 115-nm thick aluminum (Al) coplanar waveguide, 5-nm thick Al_2O_3 and dielectric isolation SiO_2 layer from the bottom to the top. As shown in Figure 1(d), the V_B^- spin defect structure contains a boron atom bombarded out of the lattice and a captured electron. Figure 1(e) displays a schematic diagram of the energy level structure of V_B^- defects.

Figure 2 (a) and (b) show the PL images of RDCs with 0-nm and 50-nm SiO_2 dielectric layers (hereafter referred to as 0-nm RDC and 50-nm RDC, respectively) and the latter is observably brighter. Figure 2(c) shows the spectra of V_B^- spin defects on the SiO_2/Si substrate, 0-nm RDC substrate and 50-nm RDC substrate. The spectral peak of V_B^- defects on 50-nm RDC is ~ 10 times higher than that on SiO_2/Si . Then we explored the influence of the thickness of the dielectric layer on the enhancement effect, and the results are shown in Figure 2(d). With the increment of the thickness of the dielectric layer, the enhancement effect first increased and then decreased.

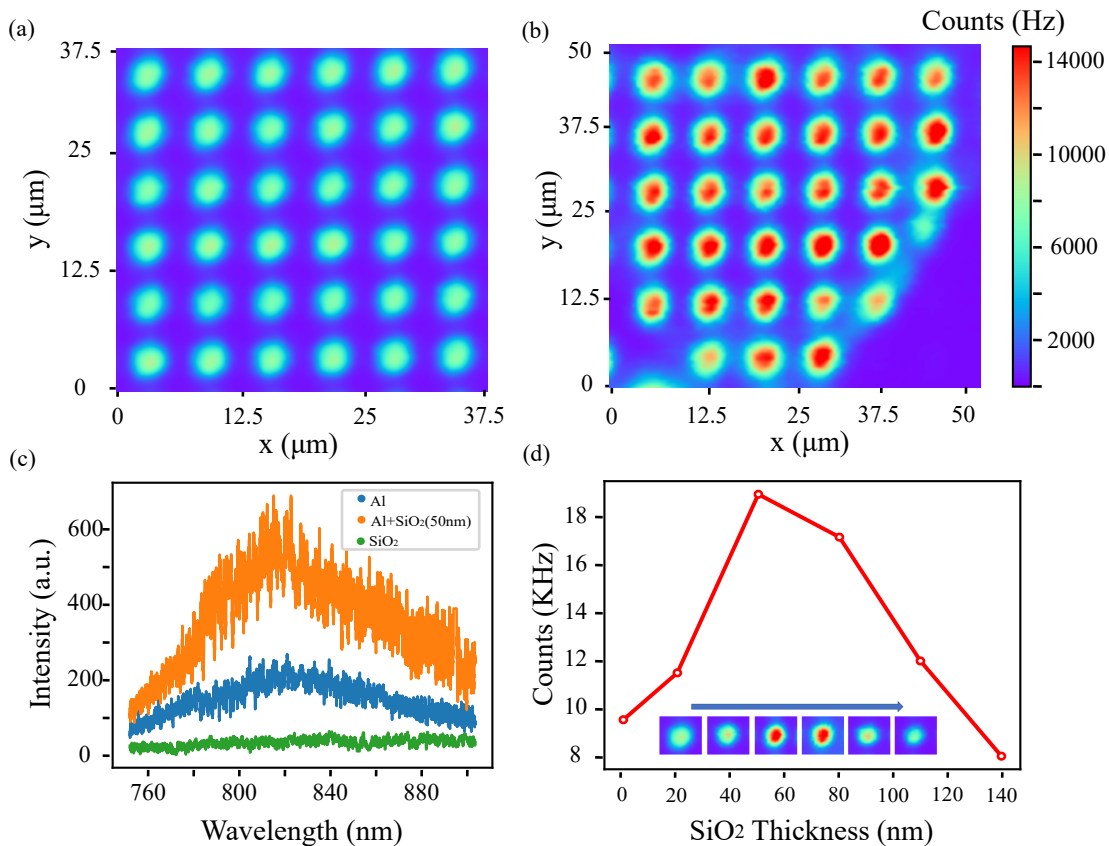


Figure 2. Optical properties of reflecting dielectric enhancement. (a) PL image of the spin defect array generated by helium ion implantation on an Al coplanar waveguide without a dielectric layer. (b) Spin defect array PL image on a 50-nm thick RDC. (c) The relative spectral intensities of different substrates under a 4 mW 532 nm laser. The measurement range is 750-900 nm. (d) The PL counts of the reflective dielectric cavity with different thick oxide layers, and the best enhancement effect was shown at 50 nm.

The results show that the enhancement effect is optimized when the thickness of the dielectric layer is 50 nm, and the fluorescence counts are enhanced approximately 7 times compared with that of the SiO₂/Si substrate.

Next, we measured the spin properties of V_B^- defects on different substrates. Using the reflective metal layer as a microwave coplanar waveguide, we can perform ODMR measurements without additional microwave radiation structures. As shown in Figure 3(a), the ODMR spectra of 0-nm RDC and 50-nm RDC both have high contrast, and for the latter, the measured ODMR contrast can reach 18%, indicating that the RDC structure has a good effect on ODMR enhancement. Furthermore, the fluorescence lifetimes of V_B^- defects on different substrates have also been measured, because the Purcell enhancement by the plasmonic effect is always accompanied by a decrement of the fluorescence lifetime. Figure 3(b) shows the fluorescence lifetime of the V_B^- emitters on 50-nm RDC and SiO₂/Si substrates. The fitted fluorescence lifetimes are 0.787 ns for the 50-nm RDC substrate and 0.825 ns

for the SiO₂/Si substrate. The lifetime of V_B^- emitters on RDC is only slightly shorter than that of V_B^- emitters on SiO₂/Si, indicating that the Purcell enhancement effect is weak and not the major effect in our experiment.

To gain a deeper understanding of the physical mechanism of the enhanced RDC substrate, we performed a numerical simulation of the RDC structure. Figure 4(a) shows the simulation results of the Purcell enhancement factor of a broadband dipole source in the reflective dielectric cavity model. The Purcell factor first increases and then decreases with the increment of the thickness of the dielectric layer, and the extreme value is approximately 61 nm. RDC has a broad-spectrum enhancement effect. From Figure 4(a), we find that the RDC has a good enhancement for the entire wave packet of V_B^- . The comparison between simulated (blue dotted line) and experimental (red circle) fluorescence enhancements is shown in Figure 4(b). The experimental data basically agree with the simulated results, and we speculate that the main error may come from the inaccuracy of

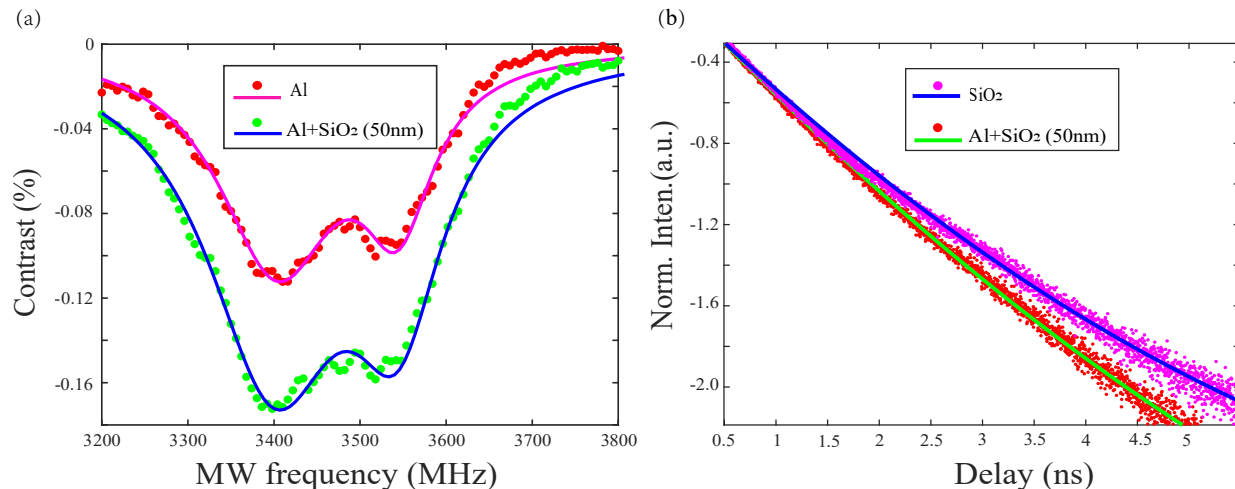


Figure 3. (a) The ODMR fitted data measured on the 0-nm RDC and 50-nm RDC. (b) The fluorescence lifetime on Si substrate and 50-nm RDC was measured. The solid lines are fitting results using $y = a * \exp(-(t - b)/\tau) + c$, and the lifetimes are 0.825 ns and 0.787 ns, respectively, showing a weak Purcell effect.

the refractive index of the dielectric layer and the incomplete approximation of the environment. Figures 4(c) and (d) are captured from the field propagation and distribution of the movie monitor in the simulation. The dissipation of spin defect luminescence on the SiO₂/Si substrate is much greater than that of the reflection dielectric cavity. The existence of a reflective metal layer reduces the loss, and results in far-field collection efficiency due to the better orientation, which provides an intuitive explanation of the reflection dielectric cavity enhancement.

Discussions

We explored the fluorescence enhancement effect and physical mechanism of the reflective dielectric cavity on the V_B⁻ defect array from the point of view of experiments and simulations. Enlarging the area of the coplanar waveguide can enhance the defects on a larger scale and be compatible with other structures. The dielectric layer can be etched as the Bragg circular resonator for hybrid enhancement [48]. It is easy to extend this enhancement structure to enhance other 2D-materials using reflective dielectric cavities. For the spin defect array produced by HIM, some points appear inhomogeneous, which we attribute to the edge effect, stress or dangling bonds or other factors. The overall uniformity of the array produced by the HIM is good. Effects such as spectral drift also exist in many enhanced structures, limiting further applications, while the spectral features of the spin-defect ensemble on hBN coupled to a reflective dielectric cavity can be well preserved.

Conclusion

Our experimental results show the enhancement of the fluorescence and ODMR contrast of the spin defect array by a reflective dielectric cavity. We explored the optimal dielectric cavity thickness and further explored the primary and secondary relationships of the enhancement related factors in combination with theoretical simulations. Since the V_B⁻ defect PL spectrum is a packet at room temperature, the reflective dielectric cavity has a good correspondence with the V_B⁻ spectrum range. This takes advantage of little enhancement to the background fluorescence, which is directly reflected in the improvement of ODMR contrast. From the simulation results, different from many enhancement structures that use a high Purcell effect to enhance the defects locally, the reflective dielectric cavity mainly uses a reflective metal layer and dielectric layer to improve the collection efficiency. Specifically, the transmission dissipation loss is reduced, and the metal reflective layer increases the upward fluorescence and is more directional. Reflection of the excitation laser by the metal reflection layer can play the role of multiple repumping. In conclusion, the reflective dielectric cavity exhibits good fluorescence and ODMR enhancement.

Method

Sample preparation. S1813 photoresist was first spin-coated on a clean SiO₂/Si substrate at a speed of 4000 rpm for 40 s and baked at 115 °C for 1 min. Then, we used standard processes of ultraviolet lithography (SUSS MABA6) and developed for 50 s to fabricate the coplanar waveguide pattern. Subsequently, we coated 120-nm aluminum film and SiO₂ dielectric layers of different thicknesses (0 nm, 20 nm, 50 nm, 80 nm, 110 nm,

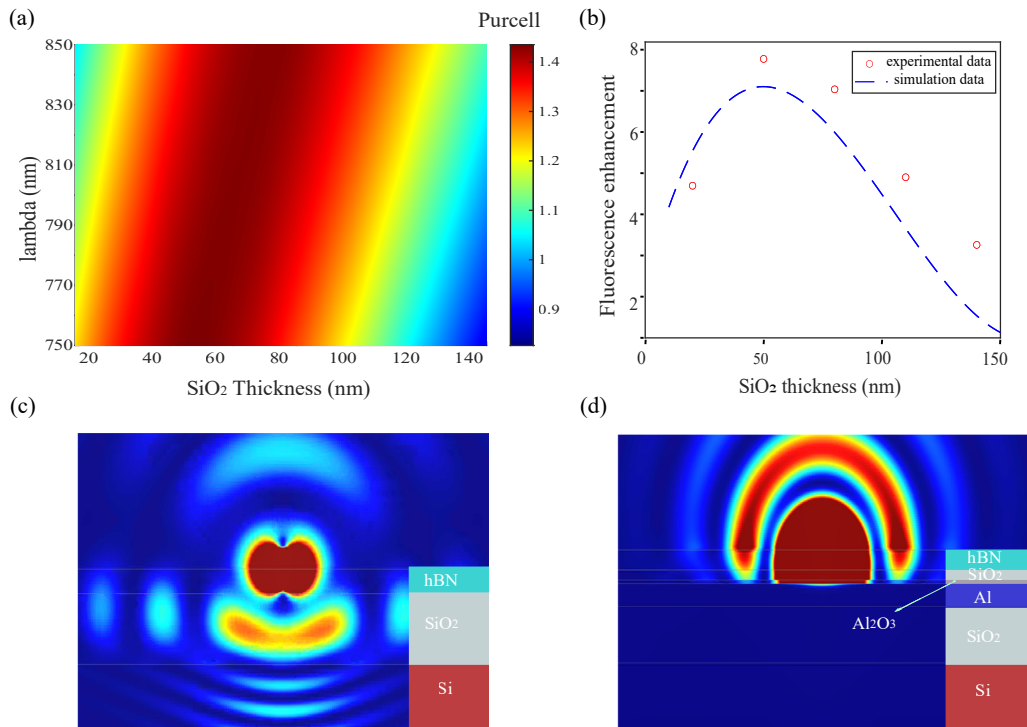


Figure 4. (a) The effect of the dielectric layer on the Purcell effect of the dielectric cavity under a wide spectrum dipole light source. We considered the oxidation effect of the Al coplanar waveguide, and set the oxide layer to 5 nm of Al₂O₃. The results show that the dielectric layer of 61 nm has the strongest Purcell effect at wavelengths of 750-900 nm. (b) The experimental and simulated PL enhancement factors of 50-nm RDC relative to the SiO₂/Si substrate. Considering the Purcell effect and the enhancement factor obtained from the simulation of the collection efficiency at a specific solid angle above the actual experimental sample, the simulation is in good agreement with the experiment. The simulation shows that the enhancement effect of the reflective medium cavity is mainly reflected in the improvement of the collection efficiency. (c) The propagation loss time slice of the dipole light source on the SiO₂/Si substrate can be visually seen to be significantly dissipated. (d) The propagation loss time slice of the dipole light source on the reflective dielectric cavity of the 50-nm -thick medium layer shows that the loss becomes weaker and the directionality in the vertical upward direction becomes better, which is the main reason for the enhancement.

140 nm) by an LAB18 E-Beam Evaporator to form the structure of RDC. Next, we transferred the hBN flake onto the RDC. Finally, we created a V_B^- spin defect by helium focused ion beam system with a 10^{17} -ions/cm² implantation dose and 30-keV implantation energy.

Simulations. All numerical simulation results are obtained using the finite difference time domain (FDTD) method, including the Purcell factor, enhancement factor, and propagation time slice diagram of the light field. The refractive index of hBN is set to 2.0, and the rest use data from the material library. The minimum mesh size is set to 0.25 μ m.

Experimental setup. We used a home-made confocal microscope with a 0.9-N.A. objective (Olympus MPLFLN100x) to measure the hBN sample. The fluorescence was excited by 532-nm laser, collected by the same objective and then reflected into the collection de-

vice through a beam splitter (BSW26R, Thorlabs) and a 750-nm long-pass filter (FELH0750 Thorlabs) to filter the laser and background fluorescence. The filtered signal light was collected using a single-mode fiber, and the fluorescence counts were detected by a silicon-based avalanche diode. For the ODMR measurement, we employed an aluminum waveguide on the substrate to transmit the microwave and used a microwave field signal generator to generate the microwave (SSG-6000RC, Mini-Circuits) and a power amplifier (ZHL-20W-13SW+, Mini-Circuits) to enhance the microwave power. In addition, we used a white light picosecond pulsed laser (SuperK Extreme, NKT Photonics) and PicoQuant for fluorescence lifetime measurement (HydraHarp).

Acknowledgments

This work is supported by the Innovation Program for Quantum Science and Technology (No. 2021ZD0301200), the National Natural Science Foundation of China (Nos. 12174370, 12174376, and 11821404), the Youth Innovation Promotion Association of Chinese Academy of Sci-

ences (No. 2017492), the Open Research Projects of Zhejiang Lab (No.2021MB0AB02), the Fok Ying-Tong Education Foundation (No. 171007). This work was partially carried out at the USTC Center for Micro and Nanoscale Research and Fabrication.

-
- [1] Sherson, J. F.; Krauter, H.; Olsson, R. K.; Julsgaard, B.; Hammerer, K.; Cirac, I.; Polzik, E. S. Quantum teleportation between light and matter. *Nature*. **2006**, *443*, 557-560.
- [2] Childress, L.; Hanson, R. Diamond NV centers for quantum computing and quantum networks. *MRS bulletin*. **2013**, *38*, 134-138.
- [3] Atatüre, M.; Englund, D.; Vamivakas, N.; Lee, S. Y.; Wrachtrup, J. Material platforms for spin-based photonic quantum technologies. *Nature Reviews Materials* **2018**, *3*, 38-51.
- [4] Awschalom, D. D.; Bassett, L. C.; Dzurak, A. S.; Hu, E. L.; Petta, J. R. Quantum spintronics: engineering and manipulating atom-like spins in semiconductors. *Science* **2013**, *339*, 1174-1179.
- [5] Togan, E.; Chu, Y.; Trifonov, A. S.; Jiang, L.; Maze, J.; Childress, L.; Dutt, M. V.; Sorensen, A. S.; Hemmer, P. R.; Zibrov, A. S.; Lukin, M. D. Quantum entanglement between an optical photon and a solid-state spin qubit. *Nature* **2010**, *466*, 730-734.
- [6] Maze, J. R.; Stanwix, P. L.; Hodges, J. S.; Hong, S.; Taylor, J. M.; Cappellaro, P.; Jiang, L.; Dutt, M. V. G.; Togan, E.; Zibrov, A. S.; Yacoby, A.; Walsworth, R. L.; Lukin, M. D. Nanoscale magnetic sensing with an individual electronic spin in diamond. *Nature* **2008**, *455*, 644-647.
- [7] Jelezko, F.; Wrachtrup, J. Single defect centres in diamond: A review. *Physica Status Solidi (a)* **2006**, *203*, 3207-3335.
- [8] Koehl, W. F.; Buckley, B. B.; Heremans, F. J.; Calusine, G.; Awschalom, D. D. Room temperature coherent control of defect spin qubits in silicon carbide. *Nature* **2011**, *479*, 84-87.
- [9] Li, Q.; Wang, J.-F.; Yan, F.-F.; Zhou, J.-Y.; Wang, H.-F.; Liu, H.; Guo, L.-P.; Zhou, X.; Gali, A.; Liu, Z.-H.; Wang, Z.-Q.; Sun, K.; Guo, G.-P.; Tang, J.-S.; Li, H.; You, L.-X.; Xu, J.-S.; Li, C.-F.; Guo, G.-C. Room temperature coherent manipulation of single-spin qubits in silicon carbide with a high readout contrast. *Natl. Sci. Rev.* **2021**, *9*, nwab122.
- [10] Caldwell, J. D.; Aharonovich, I.; Cassaboiss, G.; Edgar, J. H.; Gil, B.; Basov, D. N. Photonics with hexagonal boron nitride. *Nat. Rev. Mater.* **2019**, *4*, 552-567.
- [11] Li, S.; Thiering, G.; Udvarhelyi, P.; Ivády, V.; Gali, A. Carbon defect qubit in two-dimensional WS₂. *Nat. Commun.* **2022**, *13*, 1-7.
- [12] Cassaboiss, G.; Valvin, P.; Gil, B. Hexagonal boron nitride is an indirect bandgap semiconductor. *Nat. Photonics*. **2016**, *10*, 262-266.
- [13] Scheuer, K. G.; Hornig, G. J.; DeCorby, R. G. Polymer transfer technique for strain-activated emission in hexagonal boron nitride. *Opt. Expr.* **2021**, *29*, 26103-26115.
- [14] Mendelson, N.; Chugh, D.; Reimers, J.R.; Cheng, T.S.; Gottscholl, A.; Hu Long; Mellor, C.J.; Zettl, A.; Dyakonov, V.; Beton, P.H.; Novikov, S.V.; Jagadish, C.; Hark Hoe Tan; Toth, M.; Bradac, C.; Aharonovich, I. Identifying Carbon as the Source of Visible Single Photon Emission from Hexagonal Boron Nitride. *Nat. Mater.* **2021**, *20*, 321-328
- [15] Hayee, F.; Yu, L.; Zhang, J. L.; Ciccarino, C. J.; Nguyen, M.; Marshall, A. F.; Aharonovich, I.; Vuckovič, J.; Narang, P.; Heinz, T. F.; Dionné, J. A. Revealing multiple classes of stable quantum emitters in hexagonal boron nitride with correlated optical and electron microscopy. *Nat. Mater.* **2020**, *19*, 534-539.
- [16] Gottscholl, A.; Diez, M.; Soltamov, V.; Kasper, C.; Sperlich, A.; Kianinia, M.; Bradac, C.; Aharonovich, I.; Dyakonov, V. Room temperature coherent control of spin defects in hexagonal boron nitride. *Sci. Adv.* **2021**, *7*, 3630
- [17] Reimers, J. R.; Shen, J.; Kianinia, M.; Bradac, C.; Aharonovich, I.; Ford, M. J.; Piecuch, P. Photoluminescence, photophysics, and photochemistry of the V_B⁻ defect in hexagonal boron nitride. *Phys. Rev. B* **2020**, *102*, 144105.
- [18] Gottscholl, A.; Kianinia, M.; Soltamov, V.; Orlinskii, S.; Mamin, G.; Bradac, C.; Kasper, C.; Krambrock, K.; Sperlich, A.; Toth, M.; Aharonovich, I.; Dyakonov, V. Initialization and read-out of intrinsic spin defects in a van der Waals crystal at room temperature. *Nat. Mater.* **2020**, *19*(5), 540-545.
- [19] Guo, N.-J.; Yang, Y.-Z.; Zeng, X.-D.; Yu, S.; Meng, Y.; Li, Z.-P.; Wang, Z.-A.; Xie, L.-K.; Xu, J.-S.; Wang, J.-F.; Li, Q.; Liu, W.; Wang, Y.-T.; Tang, J.-S.; Li, C.-F.; Guo, G.-C. Coherent control of an ultrabright single spin in hexagonal boron nitride at room temperature. *arXiv (Optics)*. December 12, 2021, 2112, 2112.06191, ver. 1. <http://arxiv.org/abs/2112.06191>.
- [20] Stern, H. L.; Gu, Q.; Jarman, J.; Eizagirre Barker, S.; Mendelson, N.; Chugh, D.; Schott, S.; Tan, H. H.; Sirringhaus, H.; Aharonovich, I.; Atatüre, M. Room-temperature optically detected magnetic resonance of single defects in hexagonal boron nitride. *Nat. Commun.* **2022**, *13*, 618.
- [21] Liu, W.; Li, Z.-P.; Yang, Y.-Z.; Yu, S.; Meng, Y.; Wang, Z.-A.; Guo, N.-J.; Yan, F.-F.; Li, Q.; Wang, J.-F.; Xu, J.-S.; Dong, Y.; Chen, X.-D.; Sun, F.-W.; Wang, Y.-T.; Tang, J.-S.; Li, C.-F.; Guo, G.-C. Rabi oscillation of V_B⁻ spin in hexagonal boron nitride. *arXiv (Quantum Physics)*. January 27, 2021, 2101.11220, ver. 1. <https://arxiv.org/abs/2101.11220>.
- [22] Murzakanov, F. F.; Yavkin, B. V.; Mamin, G. V.; Orlinskii, S. B.; Mumdzhi, I. E.; Gracheva, I. N.; Gabbasov, B. F.; Smirnov, A. N.; Davydov, V. Y.; Soltamov, V. A. Cre-

- ation of negatively charged boron vacancies in hexagonal boron nitride crystal by electron irradiation and mechanism of inhomogeneous broadening of Boron Vacancy-related spin resonance lines. *Nanomaterials* **2021**, *11*, 1373.
- [23] Guo, N.-J.; Liu, W.; Li, Z.-P.; Yang, Y.-Z.; Yu, S.; Meng, Y.; Wang, Z.-A.; Zeng X.-D.; Yan, F.-F.; Li, Q.; Wang, J.-F.; Xu, J.-S.; Wang, Y.-T.; Tang, J.-S.; Li, C.-F.; Guo, G.-C. Generation of Spin Defects by Ion Implantation in Hexagonal Boron Nitride. *ACS Omega*. **2022**, *7*, 1733-1739.
- [24] Kianinia, M.; White, S.; Fröch, J. E.; Bradac, C.; Aharonovich, I. Generation of spin defects in hexagonal boron nitride. *ACS Photonics* **2020**, *7*, 2147-2152.
- [25] Gao, X.; Pandey, S.; Kianinia, M.; Ahn, J.; Ju, P.; Aharonovich, I.; Shivaram, N.; Li, T. Femtosecond laser writing of spin defects in hexagonal boron nitride. *ACS Photonics* **2021**, *8*, 994-1000.
- [26] Yang, Y. Z.; Zhu, T. X.; Li, Z. P.; Zeng, X. D.; Guo, N. J.; Yu, S.; Meng, Y.; Wang, Z.-A.; Xie, L.-K.; Zhou, Z.-Q.; Li, Q.; Xu, J.-S.; Liu, W.; Wang, Y.-T.; Tang, J.-S.; Li, C.-F.; Guo, G.-C. Laser Direct Writing of Visible Spin Defects in Hexagonal Boron Nitride. *arXiv (Optics)*. Jul 2, 2022, 2207.00714, ver. 1. <https://doi.org/10.48550/arXiv.2207.00714>.
- [27] Qian, C.; Villafañe, V.; Schalk, M.; Astakhov, G. V.; Kentsch, U.; Helm, M.; Soubelet, P.; Wilson, N.-P.; Rizzato, R.; Mohr, S.; Holleitner, A.-W.; Bucher, D.-B.; Stier, A.-V.; Finley, J.-J. Unveiling the zero-phonon line of the boron vacancy center by cavity enhanced emission. *Nano. Lett.* **2022**, *22*, 5134-5142
- [28] Ivády, V.; Barcza, G.; Thiering, G.; Li, S.; Hamdi, H.; Chou, J.-P.; Legeza, Ö.; Gali, A. Ab initio theory of the negatively charged Boron vacancy qubit in hexagonal boron nitride. *npj. Comput. Mater.* **2020**, *6*, 1-6.
- [29] Reimers, J. R.; Shen, J.; Kianinia, M.; Bradac, C.; Aharonovich, I.; Ford, M. J.; Piecuch, P. Photoluminescence, photophysics, and photochemistry of the V_B defect in hexagonal boron nitride. *Phys. Rev. B* **2020**, *102*, 144105.
- [30] Abdi, M.; Chou, J. P.; Gali, A.; Plenio, M. B. Color centers in hexagonal boron nitride monolayers: a group theory and ab initio analysis. *ACS Photon.* **2018**, *5*, 1967-1976.
- [31] Yu, P.; Sun, H.; Wang, M.; Zhang, T.; Ye, X.; Zhou, J.; Liu, H.-Y.; Wang, C.-J.; Shi, F.-Z.; Wang, Y.; Du, J.-F. Excited-state spectroscopy of spin defects in hexagonal boron nitride. *Nano. Lett.* **2022**, *22*, 3545-3549.
- [32] Mu, Z.; Cai, H.; Chen, D.; Kenny, J.; Jiang, Z.; Ru, S.; Lyu, X.-D.; Koh, T.-S.; Liu, X.-G.; Aharonovich, I.; Gao, W.-B. Excited-state optically detected magnetic resonance of spin defects in hexagonal boron nitride. *Phys. Rev. Lett.* **2022**, *128*, 216402.
- [33] Baber, S.; Malein, R. N. E.; Khatri, P.; Keatley, P. S.; Guo, S.; Withers, F.; Ramsay, A.-J.; Luxmoore, I. J. Excited state spectroscopy of boron vacancy defects in hexagonal boron nitride using time-resolved optically detected magnetic resonance. *Nano. Lett.* **2022**, *22*, 461-467.
- [34] Mathur, N.; Mukherjee, A.; Gao, X.; Luo, J.-L.; McCullian, B. A.; Li, T.-C.; Vamivakas, A. N.; Fuchs, G. D. Excited-state spin-resonance spectroscopy of V_B⁻ defect centers in hexagonal boron nitride. *Nat. Commun.* **2022**, *13*, 3233.
- [35] Liu, W.; Li, Z.-P.; Yang, Y.-Z.; Yu, S.; Meng, Y.; Wang, Z.-A.; Li, Z.-C.; Guo, N.-J.; Yan, F.-F.; Li, Q.; Wang, J.-F.; Xu, J.-S.; Wang, Y.-T.; Tang, J.-S.; Li, C.-F.; Guo, G.-C. Temperature-dependent energy-level shifts of spin defects in hexagonal boron nitride. *ACS Photon.* **2021**, *8*, 1889-1895.
- [36] Gottscholl, A.; Diez, M.; Soltamov, V.; Kasper, C.; Krauß, D.; Sperlich, A.; Kianinia, M.; Bradac, C.; Aharonovich, I.; Dyakonov, V. Spin defects in hBN as promising temperature, pressure and magnetic field quantum sensors. *Nat. Commun.* **2021**, *12*, 4480.
- [37] Lyu, X.; Tan, Q.; Wu, L.; Zhang, C.; Zhang, Z.; Mu, Z.; Pérez, J. U.; Cai, H.-B.; Gao, W.-B. (2022). Strain Quantum Sensing with Spin Defects in Hexagonal Boron Nitride. *Nano. Lett.* **2022**, <https://doi.org/10.1021/acs.nanolett.2c01722>, Chusheng Zhang, Zhaowei Zhang, Zhao Mu, Jesús Zúñiga*, Hongbing Cai*, and Weibo Gao
- [38] Healey, A. J.; Scholten, S. C.; Yang, T.; Scott, J. A.; Abrahams, G. J.; Robertson, I. O.; Hou, X.-F.; Guo, Y.-F.; Rahman, S.; Lu, Y.; Kianinia, M.; Aharonovich, I.; Tetienne, J. P. Quantum microscopy with van der Waals heterostructures. *arXiv (Mesoscale and Nanoscale Physics)*. Dec 7, 2021, 2112.03488, ver. 1. <https://doi.org/10.48550/arXiv.2112.03488>.
- [39] Huang, M.; Zhou, J.; Chen, D.; Lu, H.; McLaughlin, N. J.; Li, S.; Alghamdi, M.; Djugba, D.; Shi, J.; Wang, H.-L.; Du, C.-R. Wide Field Imaging of van der Waals Ferromagnet Fe₃GeTe₂ by Spin Defects in Hexagonal Boron Nitride. *arXiv (Materials Science)*. Dec 27, 2021, 2112.13570, ver. 1. <https://doi.org/10.48550/arXiv.2112.13570>.exagonal Boron Nitride. *Nano Letters*.
- [40] Mendelson, N.; Ritika, R.; Kianinia, M.; Scott, J.; Kim, S.; Fröch, J. E.; Gazzana, C.; Westerhausen, M.; Xiao, L.; Mohajerani, S. S.; Strauf, S.; Toth, M.; Aharonovich, I.; Xu, Z. Q. Coupling spin defects in a layered material to nanoscale plasmonic cavities. *Adv. Mater.* **2022**, *34*, 2106046.
- [41] Gao, X.; Jiang, B.; Llacsahuanga Allcca, A. E.; Shen, K.; Sadi, M. A.; Solanki, A. B.; Ju, P.; Xu, Z.; Upadhyaya, P.; Chen, Y. P.; Bhave, S. A.; Li, T. High-contrast plasmonic-enhanced shallow spin defects in hexagonal boron nitride for quantum sensing. *Nano. Lett.* **2021**, *21*, 7708-7714.
- [42] Fröch, J. E.; Spencer, L.; Kianinia, M.; Totonjian, D.; Nguyen, M.; Dyakonov, V.; Toth, M.; Kim, S.; Aharonovich, I. Coupling spin defects in hexagonal boron nitride to monolithic bullseye cavities. *Nano Lett* **2021**, *21*, 6549-6555.
- [43] Yang, T.; Mendelson, N.; Li, C.; Gottscholl, A.; Scott, J.; Kianinia, M.; Dyakonov, V.; Toth, M.; Aharonovich, I. Spin defects in hexagonal boron nitride for strain sensing on nanopillar arrays. *Nanoscale* **2022**, *14*, 5239-5244.
- [44] Fröch, J. E.; Kim, S.; Mendelson, N.; Kianinia, M.; Toth, M.; Aharonovich, I. Coupling hexagonal boron nitride quantum emitters to photonic crystal cavities. *ACS nano* **2020**, *14*, 7085-7091.
- [45] Lee, Y.-C.; Tseng, Y.-C.; Chen, H.-L. Single type of nanocavity structure enhances light outcouplings from various two-dimensional materials by over 100-fold. *ACS Photonics* **2017**, *4*(1), 93-105.
- [46] Kuo, S.-J.; Tsai, P.-C.; Lee, Y.-C.; Chang, S.-W.; So-

- toma, S.; Fang, C.-Y.; Chang, H.-C.; Chen, H.-L. Manipulating the distribution of electric field intensity to effectively enhance the spatial and spectral fluorescence intensity of fluorescent nanodiamonds. *Nanoscale* **2018**, *10*, 17576-17584.
- [47] Holewa, P.; Sakanas, A.; Gür, U. M.; Mrowiński, P.; Huck, A.; Wang, B. Y.; Musiai, A.; Yvind, K.; Gregersen, K.; Syperek, M.; Semenova, E. Bright Quantum Dot Single-Photon Emitters at Telecom Bands Heterogeneously Integrated on Si. *ACS Photonics* **2022**, *9*, 2273-2279.
- [48] Xu, S.-W.; Wei, Y.-M.; Su, R.-B.; Li, X.-S.; Huang, P.-N.; Liu, S.-F.; Huang, X.-Y.; Yu, Y.; Liu, J.; Wang, X.-H. Bright single-photon sources in the telecom band by deterministically coupling single quantum dots to a hybrid circular Bragg resonator. *Photonics Research* **2022**, *10*, B1-B6.